The Nature of Optical Features in the Inner Region of the 3C 48 Host Galaxy

Alan Stockton – University of Hawaii
Gabriela Canalizo – University of California
Hai Fu – University of Hawaii
William C. Keel – University of Alabama

Citation of published version:

Stockton, A., Canalizo, G., Fu, H., Keel, W. (2007): The Nature of Optical Features in the Inner Region of the 3C 48 Host Galaxy. *The Astrophysical Journal*, 659(1).
DOI: https://doi.org/10.1086/511952

The Astrophysical Journal, 659:195–204, 2007 April 10

THE NATURE OF OPTICAL FEATURES IN THE INNER REGION OF THE 3C 48 HOST GALAXY[1]

Alan Stockton,[2,3] Gabriela Canalizo,[4] Hai Fu,[2] and William Keel[5]

Received 2006 October 3; accepted 2006 December 15

ABSTRACT

The well-known quasar 3C 48 is the most powerful compact steep-spectrum radio-loud QSO at low redshifts. It also has two unusual optical features within the radius of the radio jet ($\sim 1''$): (1) an anomalous, high-velocity narrow-line component, and (2) a bright continuum peak (3C 48A) $\sim 1''$ northeast of the quasar. Both of these optical features have been conjectured to be related to the radio jet. We have obtained Gemini North GMOS integral field unit (IFU) spectroscopy of the central region around 3C 48. We use the unique features of the IFU data to remove unresolved emission at the position of the quasar. The resolved emission at the wavelength of the high-velocity component is peaked $\lesssim 0.25''$ north of the quasar, at the same position angle as the base of the radio jet. These observations appear to confirm that this high-velocity gas is connected with the radio jet. However, most of the emission comes from a region where the jet is still well collimated, rather than from the regions where the radio maps indicate strong disruption. We also present the results of *HST* STIS spectroscopy of 3C 48A. We show that 3C 48A is dominated by stars with a luminosity-weighted age of $\sim 1.4 \times 10^8$ yr, substantially older than any reasonable estimate for the age of the radio source. Thus, 3C 48A almost certainly cannot be attributed to jet-induced star formation. The host galaxy of 3C 48 is clearly the result of a merger, and 3C 48A seems much more likely to be the distorted nucleus of the merging partner in which star formation was induced during the previous close passage.

Subject headings: galaxies: evolution — galaxies: formation — galaxies: high-redshift

1. INTRODUCTION

3C 48 ($z = 0.369$) is a remarkable quasar quite aside from the fact that it was the first to be identified (Matthews et al. 1961; Matthews & Sandage 1963). As seems to be the case with a number of "prototypes," it is far from typical. The original identification of 3C 48 depended in part on the small size of its radio source, and 3C 48 and 3C 277.1 remain the only examples of compact steep-spectrum (CSS) radio sources among powerful quasars at redshifts <0.5. The host galaxy of 3C 48 is unusually large and bright in comparison with those of other low-redshift quasars (Kristian 1973). It is now recognized that these host galaxy properties are largely a result of a major merger (Stockton & MacKenty 1987; Canalizo & Stockton 2000; Scharwächter et al. 2004). 3C 48 was the first quasar for which an extended distribution of ionized gas was observed (Wampler et al. 1975), and it still is one of the most luminous examples of extended emission among low-redshift QSOs (Stockton & MacKenty 1987). It is one of a handful of previously identified QSOs shown by *IRAS* also to be ultraluminous IR galaxies. Star formation is currently underway at a prodigious rate in the inner part of the host galaxy (Canalizo & Stockton 2000), and there are still massive reserves of molecular gas (Scoville et al. 1993; Wink et al. 1997). All things taken together indicate that we are witnessing a brief but important phase in the history of a quasar, a time when host-galaxy star formation is near its peak, the radio jet is breaking through the dense material in the inner part of the host galaxy, and UV radiation from the central continuum source has just recently become visible along many lines of sight.

Wampler et al. (1975) noticed that the [O III] profile in 3C 48 was significantly blueshifted relative to the broad Hβ line. Higher resolution spectroscopy of the quasar (Chatzichristou et al. 1999; Canalizo & Stockton 2000) shows the reason for this apparent shift: in addition to the usual nuclear narrow-line region, there is very luminous extended high-velocity gas within about $0.5''$ of the nucleus. Chatzichristou et al. (1999) presented evidence from their integral field unit spectroscopy that the high-velocity gas has been accelerated by the interaction of the radio jet with the surrounding medium. They discussed the variation of relative line ratios, velocities, and line widths of the high-velocity and systemic-velocity components. Canalizo & Stockton (2000) found that the high-velocity gas was resolved on a slit through the nucleus at position angle -28°, with an extent of $\sim 0.5''$ and a discernible velocity gradient. But neither of these studies had sufficient spatial resolution to explore the detailed relation between the radio jet and the high-velocity gas.

Boroson & Oke (1982, 1984) long ago showed the presence of strong Balmer absorption in the 3C 48 host galaxy. Canalizo & Stockton (2000) examined the host galaxy of 3C 48 in more detail with the Keck Low-Resolution Imaging Spectrograph (LRIS; Oke et al. 1995) and showed that the spectrum of the stellar population had a classic "K+A" character. The fact that they saw Balmer absorption lines from a relatively young stellar population as well as evidence for an older population (e.g., from the Mg I *b* feature at ~ 5180 Å) meant that they could do a decomposition of the two components (using stellar synthesis models, such as those of Bruzual & Charlot 1993, 2003), and estimate, at least in a relative sense, the time that had elapsed since the end of the major starburst phase. With sufficient signal-to-noise ratio (S/N), it is possible to carry out such a decomposition

[1] Based in part on observations made with the NASA/ESA *Hubble Space Telescope*, obtained at the Space Telescope Science Institute, which is operated by the Association of Universities for Research in Astronomy, Inc., under NASA contract NAS 5-26555. These observations are associated with program GO-09365. Also based in part on observations obtained at the Gemini Observatory, which is operated by the Association of Universities for Research in Astronomy, Inc., under a cooperative agreement with the NSF on behalf of the Gemini partnership: the National Science Foundation (United States), the Particle Physics and Astronomy Research Council (United Kingdom), the National Research Council (Canada), CONICYT (Chile), the Australian Research Council (Australia), CNPq (Brazil), and CONICET (Argentina).

[2] Institute for Astronomy, University of Hawaii.

[3] Cerro Tololo Inter-American Observatory.

[4] Department of Physics and Astronomy and Institute of Geophysics and Planetary Physics, University of California at Riverside.

[5] Department of Physics and Astronomy, University of Alabama.

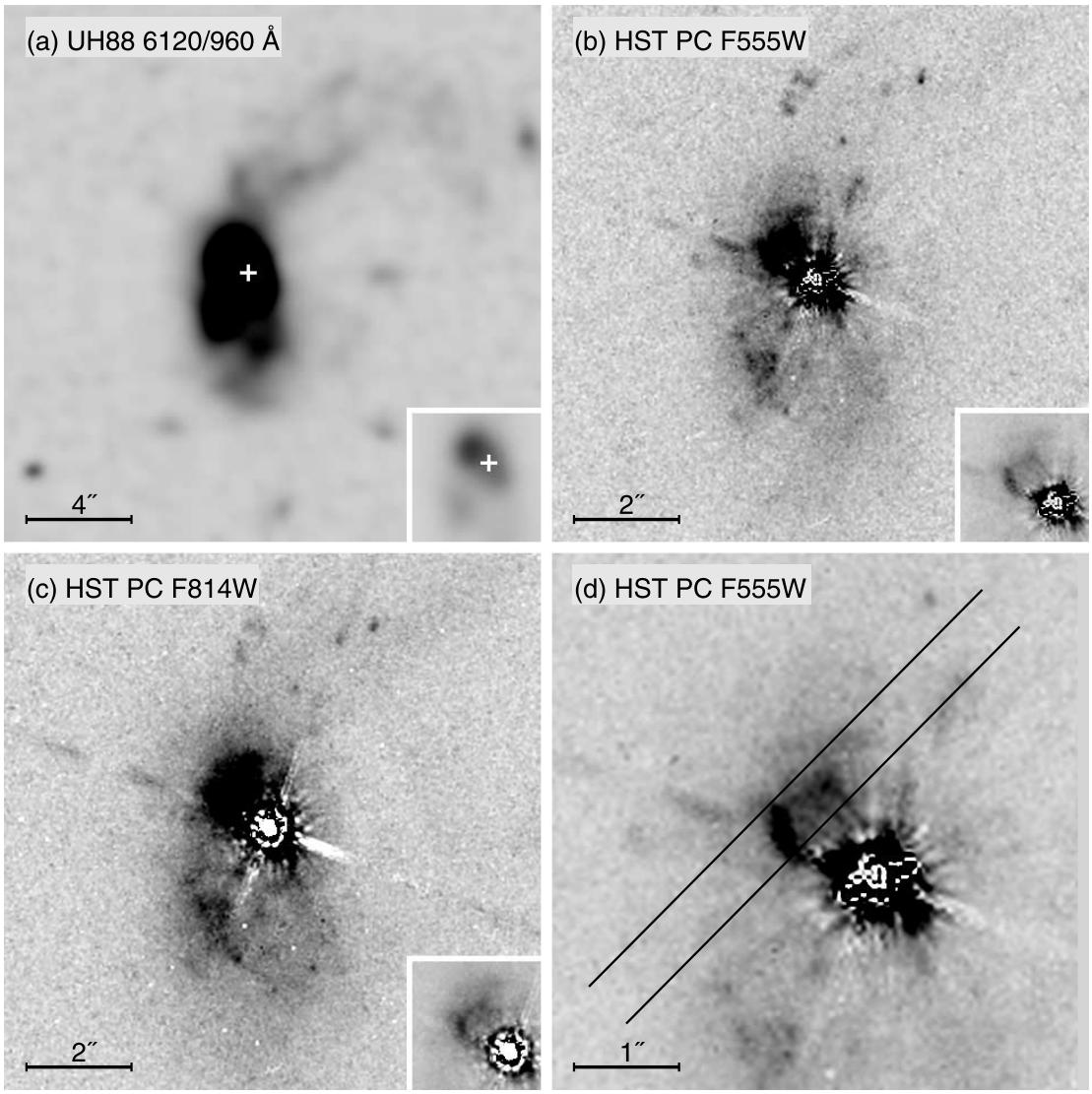

FIG. 1.—(*a*) Our deep line-free continuum ground-based image of 3C 48, after removing the quasar nucleus with the STSDAS procedure `cplucy`. The plus sign marks the position of the quasar. 3C 48A lies about 1″ NE of the nucleus (north is up and east to the left). All insets show the central region of the corresponding main panel at lower contrast. (*b*) and (*c*) *HST* PC images from the *HST* archive. The nucleus has been removed with synthetic Tiny Tim PSFs, so there are large residuals in the inner 0.5″ radius and in the diffraction spikes. The scale of these panels is enlarged by a factor of 2 from that of panel *a*. The filter bandpasses are indicated. (*d*) Enlargement (by another factor of 2) of the inner region of the *HST* PC F555W image, showing the position and width of the STIS slit.

at each point in the host galaxy, building up a map of starburst ages along lines of sight through the host galaxy (strongly weighted toward the time at which the most recent major episode of star formation ceased). Canalizo & Stockton (2000) were able to determine starburst ages and stellar radial velocities in 32 distinct regions.

But one of the most interesting features in the host galaxy was too close to the quasar to permit sufficiently low levels of contamination from quasar light to extract the galaxy spectrum. This is the luminosity peak 3C 48A ∼1″ northeast of the quasar, first noticed by Stockton & Ridgway (1991) and confirmed by subsequent ground-based and *HST* observations (Chatzichristou et al. 1999; Kirhakos et al. 1999; Boyce et al. 1999; Canalizo & Stockton 2000). One of our ground-based images is shown in Figure 1*a*, and *HST* PC images obtained from the archive are shown in Figures 1*b* and 1*c*.

Stockton & Ridgway (1991) originally suggested that 3C 48A was the secondary nucleus from a merging companion; this suggestion was consistent with the presence of the tidal tail to the northwest, as well as evidence that we are seeing the 3C 48 host galaxy near the stage of final merger (Canalizo & Stockton 2000). The attempt to model the merger by Scharwächter et al. (2004) shows that there is a short period during which the two nuclei would have a separation and position angle roughly similar to that observed for 3C 48 and 3C 48A. On the other hand, the morphology of the CSS radio jet (Wilkinson et al. 1991) and the presence of the high-velocity emission-line components near the quasar (Chatzichristou et al. 1999; Canalizo & Stockton 2000) both suggest that there is a strong interaction between the radio jet and the ambient gas in the general region of 3C 48A. 3C 48A is dominated by continuum radiation; i.e., the offset peak is seen on continuum images but not on narrowband [O III] images (Stockton & Ridgway 1991; Canalizo & Stockton 2000). However, there is no detailed correspondence between the morphology of the jet and that of 3C 48A (the jet proceeds nearly northwards rather than northeasterly), so the optical emission from 3C 48A cannot be due to synchrotron radiation. It clearly is unlikely to be nebular thermal continuum from an interaction

of the jet and the gas, because we would expect fairly strong emission-line radiation at reasonable temperatures. Chatzichristou et al. (1999) find colors for 3C 48A consistent with stars with ages similar to the likely age of the radio jet ($\lesssim 10^7$ yr). The *HST* images show that 3C 48A is curiously distorted; this distortion could result either from the shape of an overpressured region resulting from shocks from the radio jet or from the tidal stretching of the nucleus of a merging companion.

Here we use Gemini Multi-Object Spectrograph (GMOS) integral field unit (IFU) spectroscopy to analyze more precisely the position and extent of the high-velocity emission, and spectroscopy with the Space Telescope Imaging Spectrograph (STIS) on the *Hubble Space Telescope* (*HST*) to attempt to determine the nature of 3C 48A. Our principal goals for the STIS observations are (1) to determine whether the continuum radiation associated with 3C 48A is indeed due to stars; if so, (2) to determine the ages of the stellar populations involved and whether there is an age discontinuity; and (3) to measure velocities of the stellar component: do these show any evidence for distinct kinematical signature, such as might be expected if 3C 48A is the distorted nucleus of a merging companion? We assume a flat cosmology with $\Omega_m = 0.3$ and $H_0 = 70$ km s^{-1} Mpc^{-1}.

2. OBSERVATIONS AND DATA REDUCTION

2.1. *Gemini North GMOS Integral Field Unit Spectroscopy*

We obtained two-dimensional spectroscopy of the central region of 3C 48 with the integral-field mode of GMOS on the Gemini North Telescope (program ID GN-2003B-C-5). We used the half-field mode with the B600 grating, which gave a field of $3.3'' \times 4.9''$ and a wavelength range of 4318–7194 Å. The lenslets have a width of $0.2''$, and the CCD pixels correspond to $0.05''$. The total exposure was 9000 s, obtained as five 1800 s exposures. Observations of the spectrophotometric standard star G191B2B provided the flux calibration.

The raw spectral images were processed with the standard Gemini IRAF routines to give the flux calibrated data cube. The 6256 spatial planes of the data cube have dimensions of 66×98 pixels ($0.05''$ square) and are spaced at intervals of 0.46 Å. This data cube still suffers from the effects of atmospheric dispersion. Since the quasar was included within the field of view, we were able to determine its centroid for each spatial plane of the data cube. We fitted a low-order cubic spline curve to the plot of each of the coordinates as a function of wavelength and used these to generate correction offsets for each plane of the data cube. Applying these corrections generated a new data cube for which all of the image planes were correctly registered. The field of view for which the full range of wavelengths is available is, of course, somewhat smaller than the nominal field because of the atmospheric dispersion. This corrected data cube was used for analysis when we had to deal with a large wavelength range. However, for our detailed analysis of the [O III] profile, we used the uncorrected data cube, as described in § 3, in order to avoid unnecessary interpolation. The final image resolution at 6800 Å (near redshifted [O III]) was $0.55''$ (FWHM).

2.2. *HST STIS Spectroscopy*

The STIS spectroscopy was carried out with the G430L grating, covering a nominal region from 2900 to 5700 Å. The slit was centered at a position $0.97''$ east and $0.50''$ north of the quasar, at a position angle of 44.74°. The efficiency decreases quite drastically toward the UV end of the spectrum, and the useful spectral range for our project was restricted to 3630–5685 Å. Because of the low surface brightness of 3C 48A, we used the $0.5''$ slit and binned by two pixels in the dispersion direction, obtaining a total of 21,076 s of integration over eight orbits. The spectra were dithered over four positions along the slit. The slit position, superposed on the *HST* PC F555W image, is shown in Figure 1*d*. We also obtained 626 s of integration on the quasar itself with the same configuration, but without binning.

Each of the eight individual spectra of 3C 48A was first given a preliminary cleaning of cosmic rays with LACOS_IM (van Dokkum 2001). A few additional cosmic rays and other blemishes were masked manually. Masks from both the automatic and manual cosmic-ray detection for each frame were combined with dead- and hot-pixel masks generated from all of the frames. The dithered spectra and the corresponding frame masks were then shifted to a common position and coadded, using the IRAF task IMCOMBINE with CCDCLIP rejection (in addition to rejection of masked pixels). The background, including an estimate of the stellar background in the 3C 48 host galaxy, was removed by subtracting a linear fit to regions on either side of 3C 48A. The background level amounted to roughly a third of the total extracted flux in our spectral aperture, and we estimate that its scaling is accurate to ~20%. The spectrum of the brightest part of 3C 48A was extracted, using a region of six pixels ($0.3''$) wide. Some of the remaining noise spikes were removed by fitting a 160 piece cubic spline to the spectrum and rejecting points more than 2 σ away from the fit. The redshift was roughly determined from the [O II] λ3727 doublet, and the spectrum was reduced to the approximate rest frame. This redshift was corrected to a final value from fits to the stellar absorption-line spectrum.

3. THE DISTRIBUTION OF EXTENDED EMISSION IN THE NUCLEAR REGION

A full analysis of the emission over the field will be presented elsewhere; here, we concentrate only on emission very close to the quasar. For extracting spectra from our atmospheric-dispersion-corrected GMOS IFU data cube, we define 13 apertures: one centered on the quasar, and two sets equally spaced on circles around the quasar at position angles 0°, 60°, 120°, 180°, 240°, and 300°. The inner circle has a radius of $0.4''$, and the outer circle has a radius of $1.1''$; the inner apertures are labeled A0, A60, A120..., and the outer apertures are labeled B0, B60..., where the numerical part of the designation indicates the position angle of the aperture center from the quasar. All of the apertures were Gaussian weighted and were truncated at the FWHM of the Gaussian profiles, which was set to $0.4''$. We show the spectra of the quasar and the outer (B) ring of apertures in Figure 2.

It was not possible to correct the off-nuclear spectra in Figure 2 for scattered light from the nucleus because of the uncertain variation of the scattered contribution with wavelength. However, we can make this correction (with typically about 20% accuracy) for the region in the immediate vicinity of Hβ by subtracting a version of the quasar spectrum scaled to eliminate the broad Hβ line in the residual. We show the region of Hβ and [O III] $\lambda\lambda$4959, 5007 lines after this subtraction for our six off-nuclear B apertures (centered $1.1''$ from the quasar) in Figure 3 (*left panel*), as well as the same region for the quasar. In the right panel of Figure 3, we show similarly subtracted spectra for the A apertures (centered $0.4''$ from the quasar).

For the apertures at $1.1''$ radius (left panel in Fig. 3), the high-velocity component shows up most strongly in the B0 and B60 apertures; it is essentially completely absent in the B180, B240, and B300 apertures. There is a clear velocity offset of the high-velocity component between the B0 and B60 apertures, as well as evidence for more than two velocity components in the

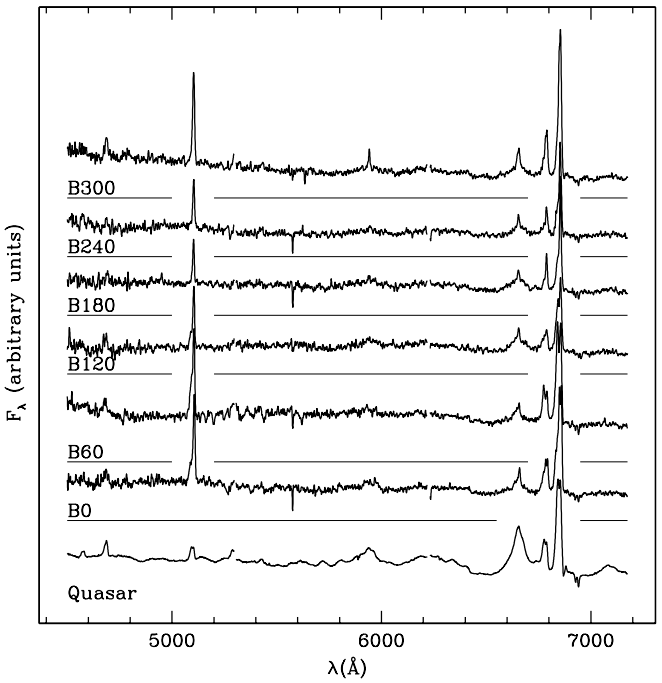

FIG. 2.—Spectra extracted from the GMOS IFU data cube, as described in the text. The quasar spectrum, shown at the bottom, has been scaled by a factor of 0.018 to roughly match the other spectra, which are all on the same scale relative to each other. The spectra are shifted for clarity, with zero levels being indicated by the horizontal lines. The off-nuclear spectra are all centered 1.1″ from the quasar at the position angles indicated. No attempt has been made to correct for scattered light from the quasar. The two slight gaps in each spectrum correspond to the gaps between the CCD detectors, and the negative feature in some of the spectra at 5577 Å is due to imperfect subtraction of the strong airglow line at that wavelength.

former. The high-velocity emission is much stronger in the inner apertures, particularly the A0 aperture, where the flux has over 10 times the highest value that it has in any of the outer apertures. It is absent from the A120, A180, and A240 apertures, but present in the A60 and A300 apertures. For this inner ring of apertures, the aperture boundaries are adjacent to each other, so there will be unavoidable spill-over because of the 0.55″ FWHM seeing disk.

At first sight, it may appear that there is a problem with the subtraction procedure because of negative [O III] residuals, particularly in the A180 spectrum. Note, however, that these negative excursions are only at the wavelength of the high-velocity component. The explanation is almost certainly that the quasar aperture encompasses high-velocity emission slightly extended to the north, which is then excess to the scattered nuclear quasar contribution to apertures on the south side.

In order to explore the spatial distribution of the high-velocity material in more detail, we analyze the image planes of the data cube as we step across the [O III] line profile. Since we are here concentrating on a very small range of wavelengths around the [O III] λ5007 emission complex, we can use the original data cube, uncorrected for atmospheric dispersion, thus avoiding any smearing from subpixel interpolation. The maximum shift due to dispersion was confirmed to be <0.1 pixel ($= 0.005''$) over this wavelength range. The general approach is this: we use the continuum on either side of the [O III] λ5007 line to precisely define the point-spread function (PSF) of the quasar; we bin narrow wavelength intervals to form images from the data cube as we step across the line profile, and we then subtract a scaled PSF from each of these to show the distribution of extended emission close to the quasar for each part of the line profile.

In more detail, we used narrow regions of continuum ($\sim$20 Å wide) immediately on either side of the emission line to define the PSF centroid at the line, but we used wider ($\sim$100 Å) continuum regions somewhat farther away to obtain better S/N for

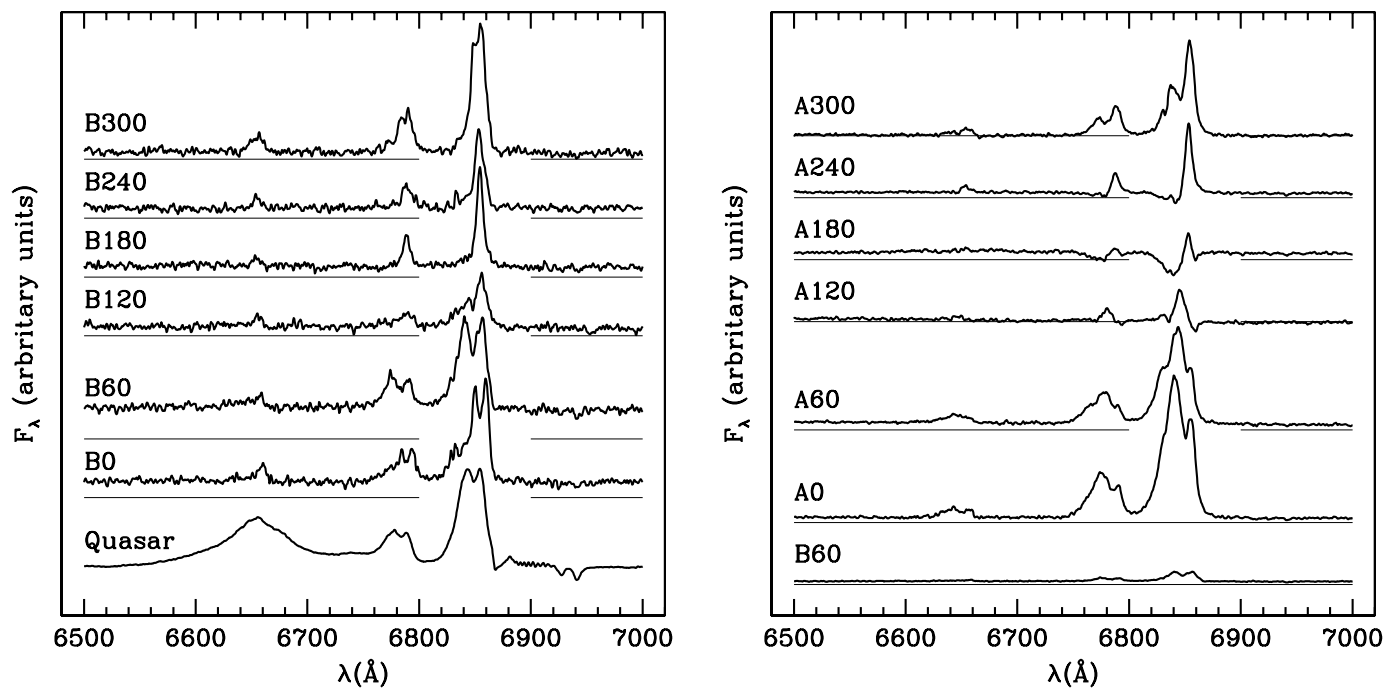

FIG. 3.—*Left*: Spectra of the region around the Hβ and [O III] $\lambda\lambda$4959, 5007 lines for the same apertures as are shown in Fig. 2; but in this case, a scaled quasar spectrum has been subtracted from each of the off-nuclear spectra to remove the scattered quasar light, as judged by the broad Hβ emission. *Right*: Similar quasar spectra for apertures at a radius of 0.4″ from the quasar. The B60 spectrum at the bottom, shown at the same scale as the other spectra, indicates the relative scaling for the two panels.

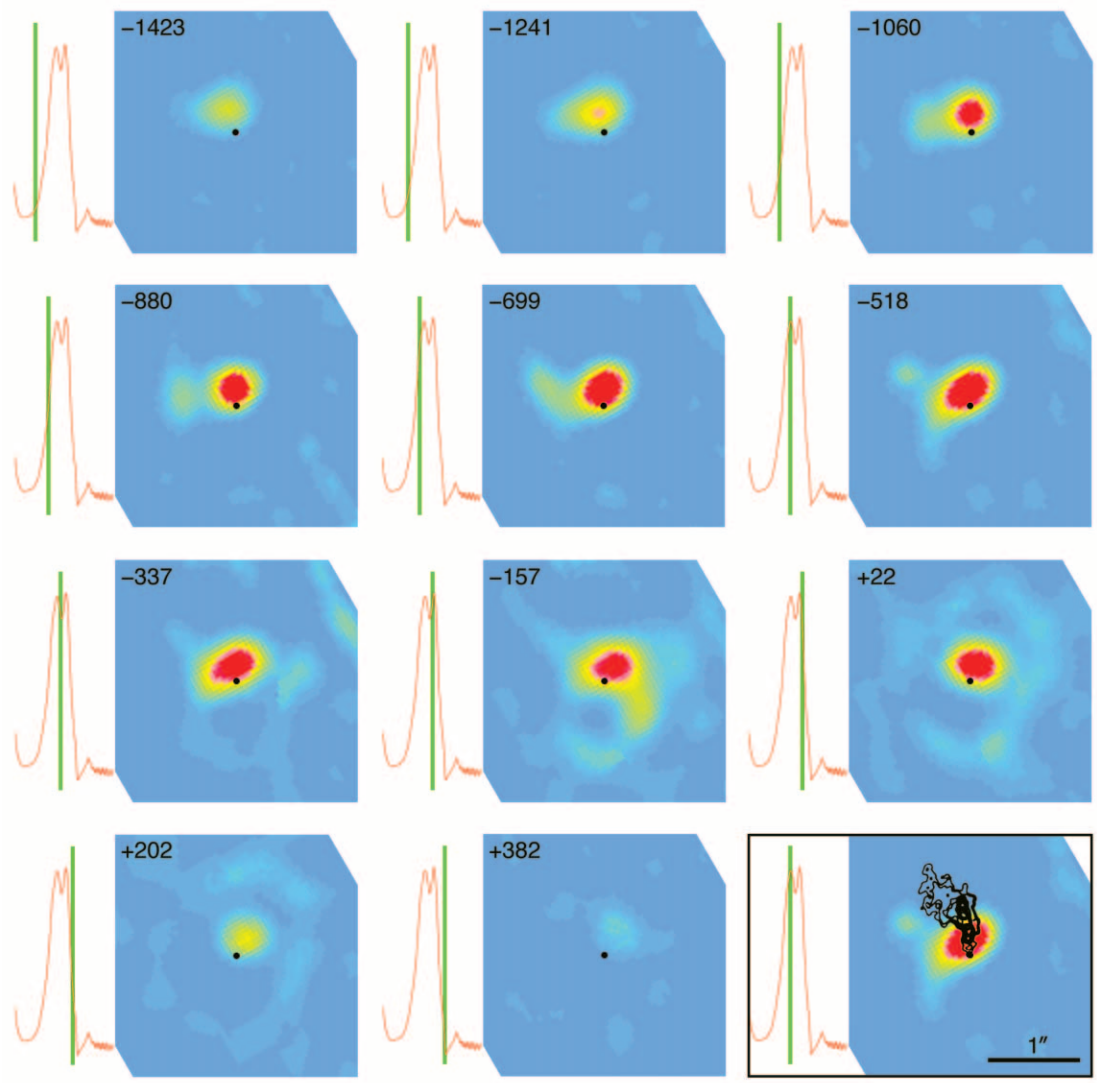

FIG. 4.—Location of nuclear [O III] extended emission in 3C 48. The unresolved nuclear emission component has been removed from these images using PLUCY (Hook et al. 1994), where the PSF has been determined from the average continuum profile on either side of the [O III] line. The black dot marks the position of the quasar. The [O III] line profile is shown to the left of each image, and the green bar indicates the wavelength region that has been summed to form the corresponding image. The number in the upper left corner of the images gives the central velocity shift of the image, in km s^{-1} in the quasar frame, from the systemic redshift of 0.36933. The 5 GHz Merlin radio contours from Feng et al. (2005) are shown superposed on the image near the peak of the high-velocity system in the lower right panel. All images use a common intensity mapping and have north up and east to the left.

the PSF profile itself. This high S/N PSF was then carefully registered (at the subpixel level) to the PSF at the emission-line wavelength. We used 11 4.6 Å wide slices to span the double-line profile. For each of these images, we ran the two-component deconvolution task PLUCY (Hook et al. 1994). Briefly, PLUCY allows separate treatment of point sources (which can be removed) and a variable background component, which is deconvolved via the Richardson-Lucy algorithm, subject to an adjustable entropy constraint. The result was that any unresolved nuclear emission (i.e., that having a distribution indistinguishable from that of the quasar continuum) was removed, and only extended emission was retained in the residual images. These images are shown in Figure 4, along with the location in the line profile each represents. We also show the radio jet (Feng et al. 2005) at the same scale.

What is immediately clear is that the high-velocity emission is concentrated to the north of the quasar, precisely in the initial direction of the radio jet, and mostly within the region where the jet appears relatively unperturbed. There is some slight variation in the position and shape of the distribution of emission across the high-velocity line profile, and there is a tail of emission at high velocities to the east, but the main emission peak remains closely aligned with the radio jet. As the wavelength window shifts toward the systemic redshift, the centroid of the extended emission moves more to the west, and more low surface brightness extended emission at greater distances becomes visible, including a possible ring of emission at about 1″ radius from the quasar. Our decomposition of the profile indicates that the narrow-line emission component at the systemic velocity is dominated by the high-velocity component at all points in the composite profile. The contribution of the systemic component is greatest (almost 50%) near its peak, but it drops off sharply at higher (as well as lower) velocities, because of the much broader velocity width of the high-velocity emission. We also expect the classical narrow-line region to be more closely centered on the nucleus and to be mostly unresolved. Reconstruction of the line profile from the deconvolved, PSF-subtracted images tends to bear out this expectation, although some residual systemic narrow-line emission still remains, perhaps indicating that this region is

slightly resolved (see also the profile in the A0 aperture in Fig. 3). However, the shift in the centroid of the emission must still largely be due to a gradient in the high-velocity component, rather than any extension of the classical narrow-line region.

From an aperture that includes essentially all of the high-velocity emission, our decomposition of the [O III] profile gives a value of 491 ± 40 km s^{-1} for the velocity offset between the two systems in the rest frame of the quasar. The [O III] fluxes in the two components are 2.9×10^{-13} and 4.1×10^{-14} ergs s^{-1} cm^{-2}, respectively, for the high-velocity and systemic-velocity components; i.e., the high-velocity gas has $\sim$7 times the [O III] luminosity of that of the classical narrow-line region.

We have attempted to estimate contributions to the Hβ profile from these two narrow-line components. We take the best-fitting Gaussian decomposition of the [O III] profile, shift these to the appropriate positions and widths for Hβ at the same redshifts, and scale the two components independently to obtain the maximum subtraction consistent with a smooth and fairly symmetric core for the Hβ residual. This procedure gives a narrow-line Hβ/[O III] ratio of $\sim$0.1 for the systemic-velocity component and $\sim$0.08 for the high-velocity component.

We have also carried out decompositions of the [O II] λ3727 doublet and the [Ne V] λ3425 line. The [O II] case is complicated by the uncertainty in the density-dependent doublet line ratio for each of the components, but the formal best fit gives a line ratio at or near the low-density limit and a total flux $\sim$16% of that of [O III] λ5007 for the high-velocity component and a line ratio near unity (indicating an electron density of a few hundred per cm^3) and a total flux $\sim$25% of that of [O III] λ5007 for the component at the systemic velocity. For the [Ne V] line, the high-velocity and systemic components have fluxes around 14% and 20% of those of their respective [O III] profiles. Our ratios for the two velocity systems for Hβ/[O III] and [O II]/[O III] are quite consistent with those reported by Chatzichristou et al. (1999). All in all, the ionization parameters of the two components seem roughly similar.

From our estimate of the Hβ flux in the high-velocity component, and assuming an electron density and temperature, the mass of the ionized gas in this component is given by

$$M_{\rm H} = \frac{4\pi m_p f_{{\rm H}\beta} d_L^2}{\alpha_{{\rm H}\beta} n_e h\nu},$$

where m_p is the proton mass, d_L is the luminosity distance, $\alpha_{{\rm H}\beta}$ is the effective recombination coefficient for Hβ, and $h\nu$ is the energy of an Hβ photon (Osterbrock 1989). The recombination coefficient is roughly an inverse linear function of temperature over the relevant temperature range; by assuming $T_e = 10^4$ K, we are unlikely to be in error from this parameter by more than a factor of 2.

If we now assume that $n_e \approx 100$ cm^{-3} and use the Hβ flux derived from the Hβ/[O III] ratio found above, we obtain $M_{\rm H} = 7.4 \times 10^8\ M_\odot$. This is likely a fairly firm lower limit to the total mass. Densities much higher than 100 cm^{-3} would be inconsistent with our fit to the [O II] λ3727 profile. It remains quite possible, however, that most of the mass of the gas could have a density <10 cm^{-3}, as it appears to be the case, for example, in the extended emission region around 4C 37.43 (Stockton et al. 2002). If this is true for the high-velocity gas associated with 3C 48 its total mass could be as much as $10^{10}\ M_\odot$.

Masses in this range can pose interesting constraints on acceleration mechanisms. The high-velocity gas is centered at a projected distance $\lesssim$1 kpc from the quasar with a differential radial velocity of $\sim$500 km s^{-1}. Wilkinson et al. (1991) argue that the weakness of the central radio component in 3C 48 means that the radio axis is likely closer to the plane of the sky than to the line of sight. In this case, the projected distance will be essentially the physical distance, and the radial velocity will be a lower limit to the space velocity. Interestingly, Gupta et al. (2005) find C IV λ1549 absorption at $z = 0.3654$ in the spectrum of 3C 48, which corresponds to a radial velocity difference in the quasar frame of 780 km s^{-1}. Thus, it would be reasonable to use $\sim$800 km s^{-1} as a lower limit to the propagation speed of the radio plasma through the ambient medium. A plausible lower limit to the kinetic energy of the high-velocity gas is then $E_K \gtrsim 6.4 \times 10^{57} M_9 v_{800}^2$ ergs, where M_9 is the mass of the high-velocity gas in units of 10^9 solar masses, and v_{800} is the bulk average velocity of the gas, relative to the quasar, in units of 800 km s^{-1}. Wilkinson et al. (1991) estimate the total energy of the radio plasma as $>10^{58}$ ergs, so the kinetic energy of the gas may account for a significant fraction of the original energy of the jet. In this case, it is clear that the gas can exert a major influence on the development of the jet, as Wilkinson et al. (1991) and Feng et al. (2005) infer from the morphology of the jet itself. Nevertheless, it is significant that most of the high-velocity gas is closer to the quasar than the region where the radio jet appears to be disrupted.

4. THE SPECTRUM OF 3C 48A

The final STIS spectrum of the high surface brightness arclike structure in 3C 48A is shown in Figure 5. As had been indicated by a comparison of broadband and [O III] *HST* WFPC imaging, the feature is dominated by continuum radiation, although some [O II] λ3727 emission is present. A prominent Hδ absorption line, seen at the long-wavelength end of the spectrum, together with a minimum in the continuum near the Balmer limit, suggests that the continuum is largely due to moderately early-type stars. Fits of spectral synthesis models confirm this conclusion. The absorption-line redshift, heavily dependent on Hδ, is 0.3693 ± 0.0002. In Figure 5 (*left panel*), we overplot on the spectrum Bruzual & Charlot (2003) solar-metallicity instantaneous-burst models with ages ranging from 100 to 200 Myr, which appear to bracket the luminosity-weighted average age of the stars. The best fit, judged by the slope of the continuum shortward of the Balmer limit, is about 140 Myr.

We have explored the possibility of younger stellar ages, combined with internal reddening, as a means of trying to fit the observed spectrum. The fundamental difficulty with this approach is the rapid decrease in the amplitude of the Balmer-limit break at ages below 100 Myr, as shown in the right panel of Figure 5. Because of the short wavelength interval involved (from $\sim$3600 to $\sim$4000 Å), the break cannot be significantly enhanced by reddening without doing unacceptable violence to the rest of the spectrum, and this conclusion holds for any plausible reddening law. It has previously been noted (see, e.g., Chatzichristou et al. 1999) that our particular line of sight to 3C 48 must have little or no significant reddening, in spite of the evidence for a major starburst in the host galaxy, and this conclusion seems to hold for 3C 48A as well, in spite of suggestions to the contrary by Zuther et al. (2004).

The fact that there is some evidence for a Ca II K line stronger than our models give encouraged us to try combinations of an old stellar population with a younger one. Such a composite population might be expected to allow a younger age for the young population. (Recall, however, that the host galaxy background

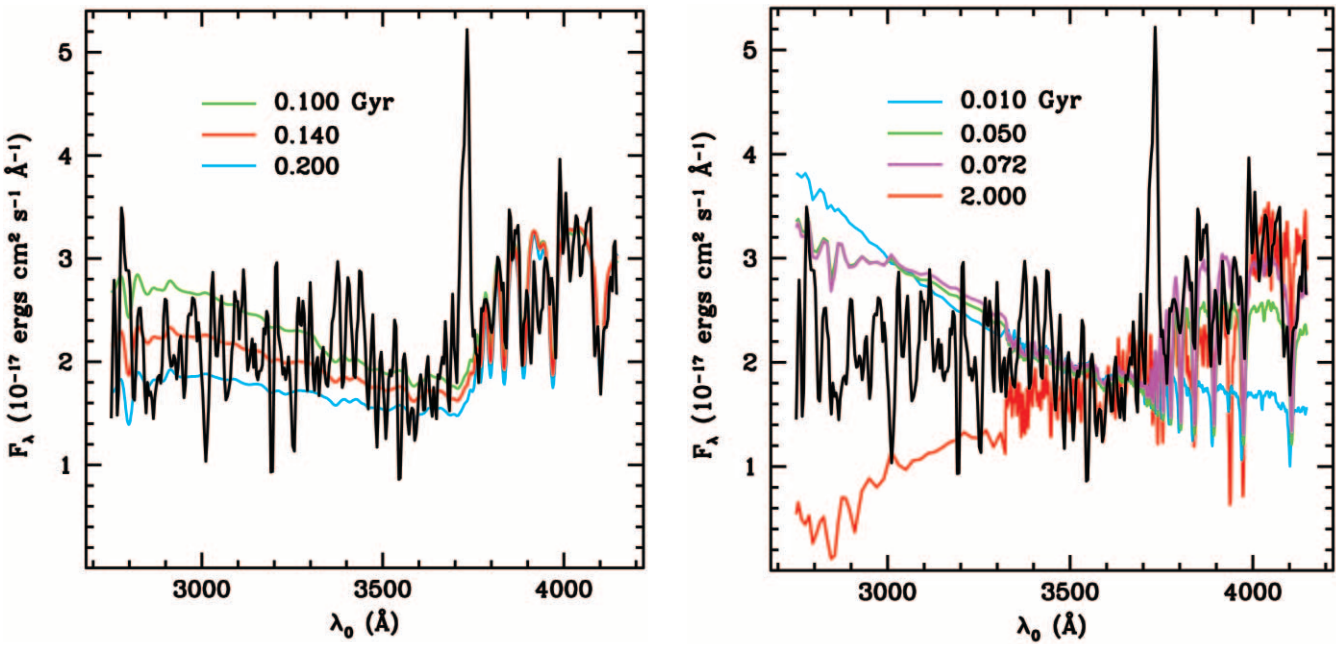

FIG. 5.—Both panels show the *HST* STIS spectrum of 3C 48A (*black trace*). The left-hand panel shows a 140 Myr Bruzual & Charlot (2003) instantaneous-burst spectral synthesis model (*red trace*), and the green and blue traces show 100 and 200 Myr models, respectively. The right-hand panel shows a range of more extreme models with ages from 10 Myr (which would be consistent with an estimate of the upper limit to the age of the stellar population in 3C 48A obtained by Chatzichristou et al. 1999) to 2 Gyr. Note that the Balmer lines and Balmer break constrain the possibility of trying to fit younger populations with substantial reddening to the data.

near 3C 48A has been subtracted off to first order by our reduction procedure, so that any significant older population would likely have to be from 3C 48A itself). The general results of these experiments are that it is difficult to add any substantial fraction (by light) of old stars without unacceptable decreases in both the Hδ strength and the Balmer break amplitude, and, even with a fairly large fraction of old stars (20% at rest frame 4050 Å), the younger component still could not be much younger than 10^8 yr.

While the difficulties of attempting to obtain a clean spectrum of 3C 48A from ground-based observations are formidable because of scattered quasar light (and particularly the difficulty of correcting for its wavelength variation), as well as contamination from other parts of the host galaxy, we were encouraged by the fact that our 60° aperture, which covers 3C 48A, shows a substantially higher continuum level than the other apertures, even in the uncorrected spectra shown in Figure 2. We tried simply subtracting a straight mean of the other five off-nuclear apertures, which are all at the same distance from the quasar. If the quasar profile is closely symmetric, this procedure should remove the scattered quasar light reasonably well. It will also, to first order, subtract the host-galaxy background, although there is certainly no guarantee that this will be very accurate, because of variations in the host galaxy surface brightness. The result is shown in Figure 6.

Naturally, one must be wary of putting too much trust in the details of this residual spectrum because of variations among the five spectra that have been subtracted from it. Nevertheless, it does agree with the general features of the STIS spectrum remarkably well, and it reinforces the conclusion that the dominant stellar population in 3C 48A must be old enough to show a substantial Balmer break.

These results are difficult to reconcile with the suggestion that 3C 48A is in some way connected with the radio jet. The fact that 3C 48A is dominated by stellar radiation eliminates any possibility that it is due to any form of gaseous emission or emission connected with relativistic electrons, such as synchrotron radiation or Compton upscattering of photons. Dust scattering of starlight from elsewhere in the host galaxy is extremely unlikely, given that the most luminous source around by far is the quasar itself, and no hint of scattered quasar radiation is seen in the STIS spectrum.

A remaining possibility is jet-induced star formation, as has been suggested by Chatzichristou et al. (1999). This now also seems unlikely because of the age of the stars. An approximate dynamical timescale for the jet can be estimated from its length and the velocity of the emission-line gas associated with

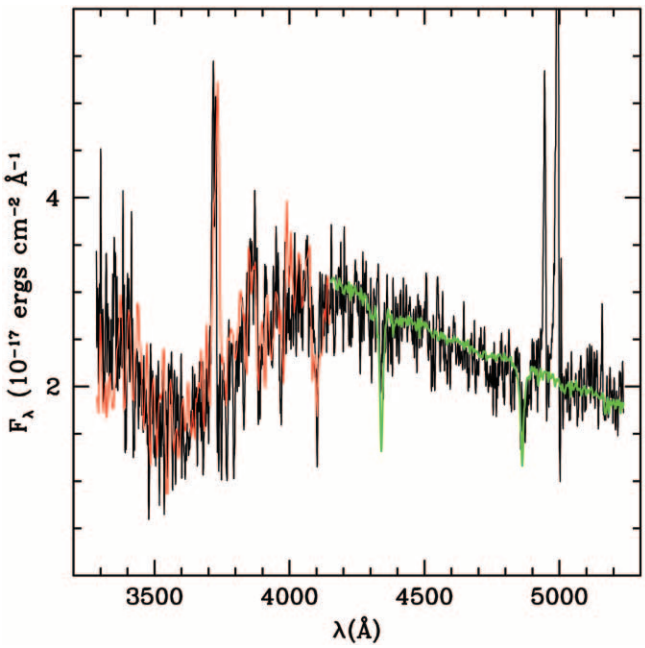

FIG. 6.—Spectra and models of 3C 48A. The black trace is the spectrum of the 60° aperture, after subtracting the mean of the other off-nuclear apertures and scaling to match the *HST* STIS spectrum, which is shown in red. The green trace is the long-wavelength portion of the Bruzual & Charlot (2003) 140 Myr model, using the same scaling as the same model in the left panel of Fig. 5.

it: $\tau_{\rm dyn} \approx 10^6 D_{\rm kpc} v_{1000}^{-1}$ yr. For $D = 5$ and $v = 0.8$ (see § 3), $\tau_{\rm dyn} \approx 6 \times 10^6$ yr. The apparent stellar age of $\gtrsim 10^8$ yr for 3C 48A is thus much older than the likely age of the radio jet. It is also much older than the likely dynamical time indicated by the distance of 3C 48A from the jet if it had been produced by it. If the arclike structure were to indicate that we are seeing the edge of a "bubble" of star formation caused by the jet, the vector from the point of origin of the bubble to the arc must likely be close to the plane of the sky. Because there is every indication that the host galaxy of 3C 48 is quite massive, yet the observed radial velocity range of the stars is quite small (Canalizo & Stockton 2000), stellar motions must be mostly in the plane of the sky. In this case, transverse velocities of at least 100 km s^{-1} must be expected for stars in this feature at $\sim$5 kpc from the quasar. This means that over 10^8 yr, we expect space motions of $\gtrsim$10 kpc, far larger than the $\sim$3 kpc observed projected separation between the end of the radio jet and 3C 48A.

Furthermore, Canalizo & Stockton (2000) had found a general trend of younger average stellar ages as one moves inward in the 3C 48 host galaxy, with stellar ages in the inner region of $<10^7$ yr, consistent with a stellar population dominated by a current starburst. 3C 48A therefore shows a clear age discontinuity with the stars in the host galaxy just slightly farther out from the center.

There is suggestive, but not conclusive, evidence for a velocity discontinuity as well. The two host-galaxy regions with absorption-line velocities in the study by Canalizo & Stockton (2000) that are closest to 3C 48A, C2 and B3 ($\sim$2″ northeast and east, respectively), have stellar velocities 173 ± 46 and 170 ± 54 higher than that of 3C 48A. Velocity gradients for the stars in central region of the 3C 48 host galaxy appear to be quite low, so this may be a significant difference.

All of this makes the possibility that 3C 48A is actually the distorted nucleus of the merging galaxy (Stockton & Ridgway 1991) seem much more attractive. An age of $\sim 10^8$ yr is not unreasonable for the time of the previous close passage prior to final merging. It is also similar to the age of star formation regions found in the leading edge of the tidal tail ($\sim$114 Myr; Canalizo & Stockton 2000), which might plausibly date from the same phase of the encounter.

5. COMPARISON WITH PREVIOUS INVESTIGATIONS OF 3C 48

The observations reported here are closely related to two previous spectroscopic studies of 3C 48 and its host galaxy that have already been mentioned: those of Chatzichristou et al. (1999) and Canalizo & Stockton (2000). We have at various points noted comparisons of our present results with these earlier studies, but it is worth discussing areas of agreement and disagreement more systematically.

Chatzichristou et al. (1999) obtained imaging spectroscopy of a $12'' \times 8''$ field around 3C 48 with an IFU consisting of 655 optical fibers, each with a diameter of 0.4″, mounted in the Multi-Object Spectrograph of the Canada-France-Hawaii telescope. The total exposure was 2700 s, and the seeing during the observation was reported to be $\sim$0.6″. The basic conclusions of this study were that: (1) the broad, blueshifted [O III] emission noticed in previous observations was actually due to a combination of the normal narrow-line region at the systemic redshift and a high-velocity component blueshifted by $\sim$580 km s^{-1}; (2) this high-velocity component dominates the [O III] profile in the center and over a region at least 0.6″ to the north and east of the quasar; (3) the location and energetics of this high-velocity gas are consistent with its having been accelerated by the radio jet; (4) the continuum colors of 3C 48A indicate dominance by a stellar population younger than 10^7 yr, with the star formation likely triggered by the radio jet; and (5) while much of the emission-line gas appears to be photoionized by the central source, there is some evidence for additional ionization from shocks.

Canalizo & Stockton (2000) were mainly concerned with stellar population distributions and ages in the host galaxy, but also discussed the emission lines present in their spectra. They obtained classical long-slit spectra with the Low-Resolution Imaging Spectrograph on the Keck II telescope, with six different slit positions. They also resolved the nuclear high-velocity component, obtaining a velocity difference from the systemic narrow-line emission of 563 ± 40 km s^{-1}. While the limitations of using slits meant that they could not effectively map its distribution, they were able to see that it had a strong velocity gradient over its extent of $\sim$0.5″ in a slit through the nucleus at position angle 333°. In agreement with Chatzichristou et al. (1999), Canalizo & Stockton (2000) also felt that the general location and velocity of this gas was strong evidence for a scenario in which it has been driven by the radio jet.

Canalizo & Stockton (2000) were not able to say anything about the stellar population of 3C 48A because scattered light from the nucleus completely dominated the spectrum in that region and could not be removed reliably, but they found quite young ages ($\sim$4 Myr, consistent with ongoing star formation) for regions in the host galaxy they could measure that were just beyond 3C 48A. On the basis of the colors reported by Chatzichristou et al. (1999) and on the morphologies of the *HST* images of 3C 48A, Canalizo & Stockton (2000) stated, "While it is still possible that this (i.e., 3C 48A) may be, in fact, the distorted nuclear regions of the companion galaxy in the final stages of merger, it now seems more likely that it, too, is related to the interaction of the radio jet with the dense surrounding medium, as suggested by Chatzichristou et al. (1999)."

The results we have given here support and refine the general conclusions of both of these previous studies regarding the high-velocity gas. With the higher resolution and better S/N of our deep IFU observations, we have been able to map out the distribution of the extended high-velocity gas in the region within $\sim$1″ of the nucleus and at several points in its velocity profile. These maps, shown in Figure 4, show that this emission peaks $\lesssim$0.25″ almost due north of the quasar, near the base of the jet, and not, as might have been expected, near the point of its obvious deflection and decollimation, roughly 0.5″ north of the quasar.

Our velocity difference between the high-velocity and systemic components of [O III] is 491 ± 40 km s^{-1}, compared with the previously reported values of 563 ± 40 km s^{-1} (Canalizo & Stockton 2000) and 586 ± 15 km s^{-1} (Chatzichristou et al. 1999). These differences are at least partly due to different approaches to calculating differential radial velocities from redshifts. Canalizo & Stockton (2000) simply treated the redshifts of the two components each as cosmological redshifts [for which $v/c = \ln(1+z)$] to find the difference in velocity, and Chatzichristou et al. (1999) apparently did the same. But since the velocity difference is actually due to bulk motion of material at essentially the same cosmological redshift as the quasar, it is more nearly correct to use the relativistic Doppler formula

$$\frac{\Delta v}{c} = \frac{(1+z_1)^2 - 1}{(1+z_1)^2 + 1} - \frac{(1+z_2)^2 - 1}{(1+z_2)^2 + 1}$$

to calculate the velocity difference. If we use this approach for the previous determinations, the Canalizo & Stockton (2000) value becomes 519 ± 40 km s^{-1}, and the Chatzichristou et al.

(1999) value becomes 537 ± 15 km s^{-1}, both of which are now consistent with our new value. (We also note that it is not clear how Chatzichristou et al. (1999) obtained their standard error of ±15 km s^{-1}, since their determination is dominated by their [O III] λ5007 velocity difference, which has a standard error of ±100 km s^{-1}. This small error may, in fact, have been a misprint, since in their "Conclusions" section, Chatzichristou et al. (1999) give the value as ∼580 ± 110 km s^{-1}).

Chatzichristou et al. (1999) had previously carried out a calculation of the total kinetic energy of the high-velocity ionized gas and compared this value with the energy available from the radio jet, similar to our calculation in § 3. The main difference in the calculations is that Chatzichristou et al. (1999) assumed a mass for the gas given by Fabian et al. (1987), which happens to agree well with the mass we obtain if the density in the emitting region is close to our approximate upper limit of $n_e \approx 100$ cm^{-3} (this agreement is mostly fortuitous, since Fabian et al. [1987] used different cosmological parameters and determined the density simply by modeling the [O III] to [O II] emission-line ratio for a single-density medium). Our lower limit to the kinetic energy is about 20% of the value (*not* intended to be a lower limit) obtained by Chatzichristou et al. (1999), so we are roughly consistent, in spite of slightly different assumptions made in the respective calculations. In both cases, the minimum energy in the high-velocity gas comprises a significant fraction of the energy of the radio jet, indicating that, if the radio jet is responsible for the current kinetic energy of the gas, the gas is quite capable of affecting the dynamics of the jet. However, especially given the fact that most of the emission occurs in a region where the jet seems relatively unperturbed, if the mass (and therefore the kinetic energy) of the gas should turn out to be significantly larger than the lower limit, it could prove to be difficult to provide sufficient energy from the radio jet alone. If this were the case, one might be forced to appeal to some other form of coupling the energy output of the quasar to the gas, the evacuation of a channel by the radio jet merely providing a convenient path for the high-velocity gas to escape. However, at this stage, such speculations are premature.

On the question of the origin of 3C 48A, we feel that our new estimate of the age of the stellar population dominating the continuum light requires a reevaluation of the previous conclusions. In our view, the balance of the evidence has swung back to the original suggestion of Stockton & Ridgway (1991) that we are seeing the distorted nucleus of the merging companion, although with the modification that most of the light is coming from stars that were likely formed from gas driven inwards during the first close pass of the interaction, some 10^8 yr earlier.

Although we believe that our *HST* STIS spectrum clearly demonstrates the dominance of stars with ages $\gtrsim 10^8$ yr, without more detailed information we can only speculate on why Chatzichristou et al. (1999) found much younger ages from their estimate of colors for 3C 48A. It seems possible that scattered light from the quasar may have had a more important influence than they had estimated. Chatzichristou et al. (1999) claimed that the scattered contribution to 3C 48A was ∼20% at 5100 Å and ∼60% at 6900 Å. We have made simple models of 3C 48 and 3C 48A using their quoted seeing of ∼0.6″. With very conservative assumptions (e.g., a Gaussian rather than a Moffat profile for the quasar), we find that the scattered contribution from the quasar would dominate that of 3C 48A by at least a factor of 2. A more realistic estimate would certainly be much larger. An additional possibility is that, with their rather large aperture centered 1.3″ from the quasar, a bit beyond the center of light for 3C 48A at 1.1″, and with ground-based seeing, the light Chatzichristou et al. (1999) measured may have been dominated by the very young stellar populations in this region of the host galaxy (Canalizo & Stockton 2000), rather than light specifically from 3C 48A. Experiments with the *HST* PC F555W image indicate that over half of the light in such an aperture (apart from scattered QSO light) would have come from host galaxy background stars rather than 3C 48A.

6. SUMMARY AND DISCUSSION

High-velocity gas associated with high-redshift radio sources has often been attributed to shocks from, or entrainment by, radio jets (e.g., Stockton et al. 1996; Solórzano-Iñarrea et al. 2001; Labiano et al. 2005; but see also Baum & McCarthy 2000). In most cases, the argument for these mechanisms has been largely circumstantial: usually, there are essentially no other plausible sources for the observed velocities. While hardly surprising, it is nevertheless gratifying to find that our high-resolution imaging strongly confirms the positional relation between the high-velocity gas and the steep-spectrum radio jet in 3C 48 found by Chatzichristou et al. (1999). Our main contribution here has been to show more clearly the distribution of the gas as a function of velocity within the profile and to show that it appears to be closely associated with the base and inner part of the jet, rather than the region farther from the quasar, where high-resolution radio maps show the most obvious deflection and decollimation.

In their two-dimensional simulations of the propagation of jets through inhomogeneous media, Saxton et al. (2005) show that it is quite plausible that CSS jets, such as that of 3C 48, do not require a direct collision with a dense cloud to suffer decollimation and deflection, as has often been assumed. Instead, the jet, in overpressuring the intercloud medium, creates shocks that propagate into and reflect off of the dense clouds. These reflected shocks can then redistribute some of the forward momentum of the jet itself into transverse components.

Saxton et al. (2005) specifically consider the case of the 3C 48 jet. They conclude that their model of a jet progressing through a medium with a rather small filling factor of dense clouds qualitatively matches the appearance of the 3C 48 jet (modulo possible differences a fully three-dimensional model might have from their two-dimensional simulations). The jet is not completely disrupted; it roughly retains its initial direction, but it is deflected through a small angle, and it becomes decollimated into a fan of material.

Taking this general picture as a working hypothesis, how does the high-velocity optical emission in 3C 48 fit in? One possibility is that it is due to shock excitation of the gas in the dense clouds responsible for decollimating the radio jet. However, our conclusion that most of the high-velocity emission comes from a region quite close to the quasar, before the jet shows significant disruption, means that the acceleration of the ionized gas is likely not closely coupled with the deflection of the jet. In addition, it is not clear that the dense clouds themselves will be accelerated to high velocities—whether they are or not depends on their size and mass distribution and the momentum transferred to them by the bow shock of the expanding radio cocoon. Insofar as we have been able to estimate the line ratios in the high-velocity component, they seem to be consistent with photoionization by the quasar continuum, as well as with ionization by shocks (at least with those for which a substantial fraction of the line radiation comes from photoionization of preshock material by the thermal continuum of the shock itself). An attractive option is that most of the emission comes from photoionization by the quasar either of ablated material from small clouds or simply of ambient diffuse gas, which likely can be driven to high velocities by the wind generated by the expanding bubble around the jet.

The possibility that 3C 48A might also be a consequence of the radio jet, in the form of jet-induced star formation, now seems rather remote. The age of the stars in this feature is incompatible with jet-induced star formation by the current radio jet, and any appeal to production by a hypothetical previous radio jet would have to explain why the feature remains so coherent and relatively close to the radio axis after $\sim 10^8$ yr. Instead, a scenario in which we are seeing the distorted nucleus of the merging companion galaxy seems much more likely. Scharwächter et al. (2004) show that a plausible model of a merger of two equal-mass disk galaxies can both reproduce the approximate appearance of the 3C 48 host and, for a brief period, place the nuclei of the merging galaxies at the separation and approximate position angle of the quasar and 3C 48A. While it would be useful to explore a larger range of parameter space to see if the model can be tuned to give a more exact reproduction of the observed properties, this result is already sufficient to give us confidence that this picture is basically correct.

These results reinforce the conclusion that we are viewing 3C 48 at a rather rare stage in the life of a quasar and its host galaxy. The age of the radio jet (which presumably also dates the triggering of the current quasar activity) appears to be at most a few 10^6 yr, and the two nuclei will fully merge on a timescale of $\sim 10^7$ yr.

Support for program GO-09365 was provided by NASA through a grant from the Space Telescope Science Institute, which is operated by the Association of Universities for Research in Astronomy, Inc., under NASA contract NAS 5-26555. We thank the referee for a very careful reading of the paper and for making numerous suggestions that materially improved the final version. The authors recognize the very significant cultural role that the summit of Mauna Kea has within the indigenous Hawaiian community and are grateful to have had the opportunity to conduct observations from it.

REFERENCES

Baum, S. A., & McCarthy, P. J. 2000, AJ, 119, 2634
Boroson, T. A., & Oke, J. B. 1982, Nature, 296, 397
———. 1984, ApJ, 281, 535
Boyce, P. J., Disney, M. J., & Bleaken, D. G. 1999, MNRAS, 302, L39
Bruzual, G., & Charlot, S. 1993, ApJ, 405, 538
———. 2003, MNRAS, 344, 1000
Canalizo, G., & Stockton, A. 2000, ApJ, 528, 201
Chatzichristou, E. T., Vanderriest, C., & Jaffe, W. 1999, A&A, 343, 407
Fabian, A. C., Crawford, C. S., Johnstone, R. M., & Thomas, P. A. 1987, MNRAS, 228, 963
Feng, W. X., An, T., Hong, X. Y., Zhao, J.-H., Venturi, T., Shen, Z.-Q., & Wang, W. H. 2005, A&A, 434, 101
Gupta, N., Srianand, R., & Saikia, D. J. 2005, MNRAS, 361, 451
Hook, R. N., Lucy, L. B., Stockton, A., & Ridgway, S. E. 1994, ST-ECF Newsl., 21, 16
Kirhakos, S., Bahcall, J. N., Schneider, D. P., & Kristian, J. 1999, ApJ, 520, 67
Kristian, J. 1973, ApJ, 179, L61
Labiano, A., et al. 2005, A&A, 436, 493
Matthews, T. A., Bolton, J. G., & Greenstein, J. L. 1961, Sky & Telescope, 21, 148
Matthews, T. A., & Sandage, A. R. 1963, ApJ, 138, 30
Oke, J. B., et al. 1995, PASP, 107, 375
Osterbrock, D. E. 1989, Astrophysics of Gaseous Nebulae and Active Galactic Nuclei (Mill Valley: Univ. Science Books)
Saxton, C. J., Bicknell, G. V., Sutherland, R. S., & Midgley, S. 2005, MNRAS, 359, 781
Scharwächter, J., Eckart, A., Pfalzner, S., Zuther, J., Krips, M., & Straubmeier, C. 2004, A&A, 414, 497
Scoville, N. Z., Padin, S., Sanders, D. B., Soifer, B. T., & Yun, M. S. 1993, ApJ, 415, L75
Solórzano-Iñarrea, C., Tadhunder, C. N., & Bland-Hawthorn, J. 2001, MNRAS, 323, 965
Stockton, A, & MacKenty, J. W. 1987, ApJ, 316, 584
Stockton, A., MacKenty, J. W., Hu, E. M., & Kim, T.-S. 2002, ApJ, 572, 735
Stockton, A., & Ridgway, S. E. 1991, AJ, 102, 488
Stockton, A., Ridgway, S. E., & Kellogg, M. 1996, AJ, 112, 902
van Dokkum, P. G. 2001, PASP, 113, 1420
Wampler, E. J., Robinson, L. B, Burbidge, E. M., & Baldwin, J. A. 1975, ApJ, 198, L49
Wilkinson, P. N., Tzioumis, A. K., Benson, J. M., Walker, R. C., Simon, R. S., & Kahn, F. D. 1991, Nature, 352, 313
Wink, J. E., Guilloteau, S., & Wilson, T. L. 1997, A&A, 322, 427
Zuther, J., Eckart, A., Scharwächter, J., Krips, M., & Straubmeier, C. 2004, A&A, 414, 919